Identification of molybdenum immobilization mechanisms in naturally contaminated excavated rocks and soils stabilized with zero-valent iron

Maxime Brandely, Samuel Coussy, Denise Blanc-Biscarat, Hicham Khodja, Rémy Gourdon

Applied Geochemistry 188 (2025) 106433

Contents lists available at ScienceDirect

Applied Geochemistry

journal homepage: www.elsevier.com/locate/apgeochem

Identification of molybdenum immobilization mechanisms in naturally contaminated excavated rocks and soils stabilized with zero-valent iron

Maxime Brandely [a,b,c], Samuel Coussy [b,*], Denise Blanc-Biscarat [a], Hicham Khodja [d], Rémy Gourdon [a]

[a] Univ Lyon, INSA Lyon, DEEP, EA7429, 69621, Villeurbanne, France
[b] Bureau de Recherches Géologiques et Minières (BRGM), 3 av. C. Guillemin, BP 36009, 45060, Orléans, Cedex 2, France
[c] Bouygues Travaux Publics, 1 avenue Eugène Freyssinet, GUYANCOURT, 78280, France
[d] Université Paris-Saclay, CEA, CNRS, NIMBE, LEEL, Gif-sur-Yvette, 91191, France

ARTICLE INFO

Editorial handling by Joann M Holloway

Keywords:
Excavated soils
Geogenic contamination
Molybdenum
Stabilization
Zero valent iron
Nuclear microprobe analysis

ABSTRACT

Chemical stabilization of naturally contaminated excavated materials could be used to limit environmental risks. Nevertheless, due to the low levels of contamination in such materials a more precise characterization of immobilization mechanisms is required. To overcome this lack of data, zero valent iron (Fe^0) was used as a stabilizing agent at rates of 1 or 3 wt% in four different sets of excavated rock and soil from the Paris basin that were contaminated with low levels of molybdenum (with a total content of from 2 to 11 mg Mo kg^{-1}) but that involved leachability issues. Molybdenum (Mo) release was reduced by at least one order of magnitude after adding Fe^0 over a wide pH range (i.e. $2 < pH < 12$). Geochemical modeling of pH-dependent leaching tests was done to identify potential immobilizing mechanisms. For Mo, experimental results were well represented at pH close to and below the natural pH of the samples by considering surface adsorption with iron (hydr-)oxides involving non-, mono- and bi-protonated Mo surface species. Zero valent iron stabilization remained relatively significant under alkaline conditions where complexation of anionic species was not favored. These results suggested that stronger binding mechanisms are likely to occur concomitantly with surface adsorption. Finally, thanks to their high sensitivity, μ-particle-induced X-ray emission (μ-PIXE) and μ-Rutherford backscattering spectroscopy (μ-RBS) were successfully used to directly observe Mo presence in iron (hydr-)oxides formed after addition of Fe^0.

1. Introduction

For major public infrastructure projects such as the Grand Paris Express (GPE) in France, the fate of trace elements (TE) in excavated rock and soil has become a key issue. The management of such materials must comply with the European Decision 2003/33/EC (OJEC, 2003), which regulates their storage in terms of leaching potential rather than total contents. In GPE construction sites, a significant proportion of excavated material contains low levels of TE but has a high leaching potential (especially regarding Molybdenum, Mo), with the concomitant environmental risk of groundwater contamination following TE release in a storage scenario. Studies have already discussed TE leachability by identifying their initial distribution in the host rocks for different types of naturally-contaminated excavated rock and soil (Tabelin et al., 2014). In the Paris basin, a high diversity has been observed, depending on the geological formation in question. Molybdenum release is higher in carbonated and clay-rich rock and soil respectively (Sterckeman et al., 2006; Cabrerizo et al., 2020; Diaz Caselles et al., 2021). Specific associations with mineral phases (pyrites, carbonates, celestite, etc.) were acknowledged, but the easiest Mo mobilization comes from weak interactions of Mo with natural iron (hydr-)oxides, clay fractions and/or carbonates (Brandely et al., 2022a).

Because of its low cost, rapidity and ease of operation, chemical stabilization has been widely used to reduce the mobility of toxic elements in a wide range of contexts (Khalid et al., 2017; Beiyuan et al., 2016). The aim of chemical stabilization is to decrease the materials' toxicity by trapping contaminants in the solid bulk (NF EN ISO 11074, 2015). The efficiency of the stabilization strongly depends on the

* Corresponding author.
E-mail addresses: maxime.brandely@cer.colas.fr (M. Brandely), s.coussy@brgm.fr (S. Coussy), denise.blanc-biscarat@insa-lyon.fr (D. Blanc-Biscarat), hicham.khodja@cea.fr (H. Khodja), remy.gourdon@insa-lyon.fr (R. Gourdon).

https://doi.org/10.1016/j.apgeochem.2025.106433
Received 26 November 2024; Received in revised form 7 May 2025; Accepted 17 May 2025
Available online 19 May 2025

physico-chemical mechanisms involved, which, in turn, depend on the type of contaminant, the selected stabilizing agent, the composition of the bulk material and the environmental conditions under which it will be exposed (Palansooriya et al., 2020). In a previous work (Brandely et al., 2022b), zero valent iron (Fe^0) showed the most promising results for mitigating Mo mobility based on standardized batch leaching tests (NF EN 12457-2, 2002).

Technologies based on zero-valent iron have been widely used for on-site or off-site remediation of soil contaminated with inorganic toxic elements such as As, Cd, Cr, Cu, Pb or Zn (Houben et al., 2012; Kumpiene et al., 2006; Hartley et al., 2004; Tiberg et al., 2016; Mench et al., 2006). The observed stabilization mechanisms involved mainly the high reactivity of Fe^0 under most environmental conditions (Guan et al., 2015). Two major types of mechanism were proposed: (i) stabilization using iron as a sorbent, involving sorption and/or (co)-precipitation phenomena with freshly formed iron (hydr-)oxides, and (ii) reductive stabilization involving electrons coming from Fe^0 oxidation to reduce contaminants into less mobile forms (Cundy et al., 2008). Regarding Mo contamination, examples of soil treatment with Fe^0 alone have not yet been reported. Recent studies have focused rather on the use of enhanced materials such as biochar or polysulfide supported nanoscale Fe^0 (Wang et al., 2021). Nevertheless, the most common forms of Mo under oxic environments, namely molybdate (MoO_4^{2-}, Mo_{VI}), are known to interact strongly with iron (hydr-)oxides with the result that Fe^0 addition has been efficiently used for treating wastewater (Vollprecht et al., 2019; Calugaru et al., 2021).

This article presents a qualitative and quantitative evaluation of the efficiency of Fe^0 addition for Mo stabilization in four different sets of excavated material from the GPE construction sites. One of the specificities of this study was the low Mo total content observed in all excavated materials (<11 mg Mo kg^{-1}). Most published studies on the subject considered higher concentrations up to 670 mg Mo kg^{-1} (Wang et al., 2021; Mancini et al., 2020). Both direct and indirect observation were used to identify the mechanisms of Mo immobilization and the behavior of Fe^0 in the solid bulk. Indirect observation involved geochemical modeling of pH-dependent leaching tests carried out on samples that were either spiked or not spiked with Fe^0 while the former involved powerful X-Ray analysis such as micro Proton Induced X-ray Emission (μ-PIXE) to circumvent detection limit issues due to the low levels of contamination.

2. Materials and methods

2.1. Samples

Four materials excavated from distinct geological formations of GPE construction sites were selected. A calcareous sample (CS) was collected in March 2018 during excavation for construction of a train station in Courbevoie (France). Almost exclusively composed of carbonated minerals, the CS came from a geological formation of the Lutetian inferior (Eocene, depth 24–27 m). A loam sample (LS) mainly composed of kaolinite and smectite-type minerals was extracted from an Ypresian inferior clay formation (Eocene, depth *c.a.* 15 m) in Clamart (France), during excavation for construction of a metro station. Finally, two argillaceous limestone samples were collected in Vitry-sur-Seine (France) either during excavation of earth for a train station (MLS-A) or during construction of diaphragm walls (MLS-B). The MLS-A sample came from an argillaceous limestone formation corresponding to Lutetian superior (Eocene, depth 13–14 m) while the MLS-B sample was extracted from a deeper formation of the Montian (Paleocene, depth 12–13 m). Although similar, MLS-A and MLS-B mineralogical compositions mainly differ in that MLS-A had a higher total content of sulfates (especially celestite, $SrSO_4$).

Molybdenum total contents were respectively 10.9 mg Mo kg^{-1} in CS, 1.6 mg Mo kg^{-1} in LS, 7.2 mg Mo kg^{-1} in MLS-A, and 2 mg Mo kg^{-1} in MLS-B. The main mineral phases of each sample of excavated material are given in Supplementary Information (SI; Table SI–1).

2.2. Chemical stabilization

The quantity of zero valent iron (Fe^0) needed to satisfy inert waste landfill acceptance criteria had been determined previously (Brandely et al., 2022b). It has been set at 3 wt% for CS and LS, and 1 wt% for MLS-A and MLS-B. The Fe^0 was provided by VWR (>98 %). An X-Ray Diffraction (XRD) analysis of the dried (38 °C) and micronized (20 μm) commercial Fe^0 was made using a Bruker D8 Advance Da Vinci diffractometer equipped with a Cu Kα radiation tube at a scanning speed of $0.03°2\theta.s^{-1}$. The diffractogram pattern in SI (Fig. SI–1) shows the almost exclusive presence of native Fe.

Chemical stabilization was done using a cutting mixer to ensure mechanical mixing for a short time of approximatively 5 min. Occasionally, and especially for the clay material (LS), a longer mixing time and manual breaking of clay blocks were needed to ensure a homogeneous mixture. Before adding Fe^0, deionized water was added to reach an optimal water content (*i.e.* the one giving the highest dry bulk density). The mass of Fe^0 to be added (m) in order to reach the desired mass percentage (W) was then calculated using:

$$m = \frac{W \times (M \times DMC)}{1 - W} \quad [1]$$

With M being the mass of material and DMC the Dry Matter Content.

2.3. pH-dependent leaching tests

The pH-dependent leaching tests protocol was adapted from the French standard (NF EN 14429, 2015) and other references (Coussy et al., 2011; Drapeau C., 2018). It was applied to both raw and Fe^0-stabilized samples. A preliminary titration was carried out on raw materials to detect the main buffer area. From these results, solutions with varying concentrations of HNO_3 or NaOH were prepared and used on previously dried (<38 °C) and crushed (<1 mm) solid samples with a Liquid/Solid ratio of 10 L kg^{-1}. The number of solutions varied from one material to another but at least 20 % were duplicated to ensure the reproducibility of the experiment. Leaching tests were carried out in plastic bottles for 72 h with agitation (60 rpm) by an end-to-end agitator. The trial duration had also been determined by a preliminary investigation of pH variations after different agitation times. Three days of agitation were needed to obtain stability in pH measurements (variations below 0.1 pH unit) inferring that a steady state had been reached. The pH range varied greatly, from 0.5 to 13 for most samples. Following agitation, supernatants were first recovered by centrifugation (3000 g, 10 min) and then filtrated (0.45 μm) before analysis. Major element concentrations were analyzed by Inductively Coupled Plasma Optical Emission Spectrometry (ICP-OES) with a Jobin Yvon Ultima 2 instrument (NF EN ISO 11885, 2009). Molybdenum concentrations were measured by Inductively Coupled Plasma – Mass Spectrometry (ICP-MS) using a THERMO X Series II instrument according to (NF EN ISO 17294-2, 2016). Anions (Chlorides - Cl^-, Fluorides - F^- and sulfates - SO_4^{2-}) were analyzed by ionic chromatography (DIONEX).

2.4. Geochemical modeling

2.4.1. General considerations for mineralogical assemblage modeling

The aim of the present study was to use the modeling approach developed for raw materials (Brandely et al., 2022a) to describe the reactivity of Fe^0-stabilized materials to pH variations with a particular emphasize on Mo behavior. This should lead to specific models being defined for the selected matrices, so that the input parameters can be reused in other studies, in line with the environmental issues relating to these matrices in the GPE project.

The geochemical model was supported by the PHREEQC software

Table 1
The modeling scenarios used to represent Mo reactivity in raw (Case 1) and Fe^0-stabilized (Case 2 and 3) materials.

	Case 1	Case 2	Case 3
Sample	Raw sample	Fe^0-stabilized sample	Fe^0-stabilized sample
Modeling Fe^0 addition	–	Fe^0 converted into Fe (hydr-)oxides	Fe^0 converted into Fe (hydr-)oxides
Surface complexation	Generalized Two Layer Model (GTLM)[a]		
Mo surface species	Non-protonated[b]: ≡Hfo_OHMoO$_4^{2-}$–Bi-protonated[b]: Hfo_OMo(OH)$_5$	Non-protonated[b]: ≡Hfo_OHMoO$_4^{2-}$–Bi-protonated[b]: Mono-protonated[a]: ≡Hfo_wMoO$_4^{2-}$	Non-protonated[b]: ≡Hfo_OHMoO$_4^{2-}$ Bi-protonated[b]: Hfo_OMo(OH)$_5$ Mono-protonated[a]: ≡Hfo_wMoO$_4^{2-}$ with **optimization** of the **formation constants** using Phreeplot software[c]
Precipitation	Control of the saturation ratio of ferromolybdate minerals: $FeMoO_4$ and $Fe_2(MoO_4)_3$		

[a] Gustafsson (2003).
[b] Dzombak and Morel (1990).
[c] Kinniburgh and Cooper (2011).

(version 3.5.0.14000; Parkhurst and Appelo, 2013) with input from the thermodynamic database Thermochimie (Giffaut et al., 2014). The database was occasionally modified by adding mineral phases that were lacking or by implementing complexation reactions to be used by the surface complexation model described below. The modeling methodology, already described in Brandely et al. (2022a), is based on three main steps: (i) integration of the mineralogical assemblages of each excavated material based on XRD results as input data, (ii) modeling of mineral assemblages and the behavior of major elements during pH-dependent leaching tests and (iii) modeling of Mo behavior. A trial and error approach was used and steps (ii) and (iii) were repeated until a satisfactory match was found between experimental and modeling results.

The solid bulk was considered through a mix of mineral phases; some were expected to react until reaching thermodynamic equilibrium within the time of the leaching test (*i.e.* carbonates, gypsum) while others (*i.e.* silicate, sulfides, celestite, iron oxides) were kinetically limited by a time and pH-dependent rate law following the approach of Marty et al. (2015). Moreover, mineral phases (*e.g.* ettringite, strontianite, brucite, and ferrihydrite) were allowed to precipitate during the batch leaching tests to represent particular features of the leaching patterns of major element. The initial quantity of all mineral phases considered for each material are given in SI (Table SI–2) and compared with the quantity suggested by XRD analysis. The dissociation reactions considered for each mineral phase as well as the corresponding thermodynamic constants are also given in SI (Table SI–3).

Complexation was only considered at metallic (hydr-)oxide surfaces since all samples were largely depleted of organic matter. In our study we chose to consider only one mineral phase per material as a surrogate for the whole pool of metallic (hydr-)oxides. In the mainly carbonated samples (CS, MLS-A and MLS-B), natural iron (hydr-)oxides were not detected by XRD so it was assumed that a fixed quantity of goethite (FeOOH) was hosting the reactive surface sites (*i.e.* equivalent to 25 wt% of total Fe). For LS, a non-negligible amount of hematite (Fe_2O_3) was detected by XRD and therefore implemented in the complexation model. The formalism of the complexation model for Mo was based on the Generalized Two Layered Model (Dzombak and Morel, 1990), which was used because it is easy to parameterize. The main characteristics of surface sites were fixed in agreement with the parameters specified by Dzombak and Morel (1990) for ferrihydrite. Two types of reactive surface sites (Hfo s and Hfo_w) were defined with surface site densities of 0.005 mol mol of Fe^{-1} and 0.2 mol mol of Fe^{-1} respectively. Specific surface areas varied depending on the iron (hydr-)oxide considered and was set to 100 $m^2\ g^{-1}$ for goethite, 12 $m^2\ g^{-1}$ for hematite and 650 $m^2\ g^{-1}$ for ferrihydrite (Hiemstra and van Riemsdijk, 1996; Yue et al., 2020; Gustafsson and Tiberg, 2015). Complexation reactions were considered regarding Mo and potentially competing major elements. The associated thermodynamic data are given in SI (Table SI–4). The competing elements were selected according to the chemistry of the different matrices studied. Phosphate (PO_4^{3-}), known for its strong interactions with iron (hydr-)oxides surfaces, was not selected as a competitor ion in these reactions, as it was not found in the samples.

Finally, Mo was incorporated in the model in two different ways. First, depending on the material considered, identified mineral phases (*i.e.* pyrite, dolomite and celestite) were assumed to bear a substantial quantity of Mo as given in SI (Table SI–5). Then, an exchangeable quantity was directly implemented in the liquid phase and allowed to equilibrate with the available surface sites. This quantity was set equal to the concentration released at the materials' natural pH (pH_{nat}).

2.4.2. Modeling Fe^0-stabilized materials

Zero-valent iron stabilization was simulated by adding iron (hydr-) oxides consistently with the actual mass of Fe^0 used during stabilization protocols. Occasionally, minor adjustments of geochemical models were performed to describe small deviations between experimental observations made on raw and on Fe^0-stabilized materials. Among these adjustments, it should be noted that the quantity of initial carbonates was slightly modified in Fe^0-stabilized CS and MLS-A to account for discrepancies in the pH buffer plateau length and that a small quantity of nontronite-like mineral was considered in Fe^0-stabilized LS. All these differences are summarized in SI (Table SI–2). The main features of modeling scenarios developed to represent Mo reactivity during pH-dependent leaching tests are given in Table 1.

2.5. Nuclear microprobe analysis

Micro Proton Induced X-Ray Emission (μ-PIXE) and Micro Rutherford Backscattering Spectroscopy (μ-RBS) analysis were simultaneously carried out using a micro-proton beam ($2 \times 2\ \mu m^2$) at 2.7 MeV and a current of 180 pA. Analyses were performed on Fe^0-stabilized CS to detect and quantify the presence of Mo on newly formed iron (hydr-) oxides following the addition of Fe^0. Carbon-coated (20 nm) polished sections were analyzed using the nuclear microprobe of the *Laboratoire d'Étude des Éléments Légers* (LEEL) in Saclay, France (Khodja et al., 2001). A preliminary Scanning Electron Microscope (SEM) investigation enabled the selection of potentially Mo-bearing iron (hydr-)oxides grains. Micro Rutherford Backscattering Spectroscopy (μ-RBS) was used to highlight the different phases located in the scanned region and to determine the composition of the major elements. Micro-Particle Induced X-ray Emission (μ-PIXE) was used to evaluate Mo trace element concentrations and limits of detection.

3. Results and discussion

3.1. Qualitative impact of Fe^0 addition on Mo leaching

Fig. 1 shows the evolution of Mo concentrations (main y-axis) during pH-dependent leaching tests of raw and Fe^0-stabilized samples. For each material, a bar graph (secondary y-axis) is also included to indicate the actual percentage of total Mo released at regular pH intervals. It should be noted that leached concentrations from stabilized samples were mainly lower than the one obtained from raw materials. Only one exception was observed in MLS-A at pH < 2, for which the stabilized

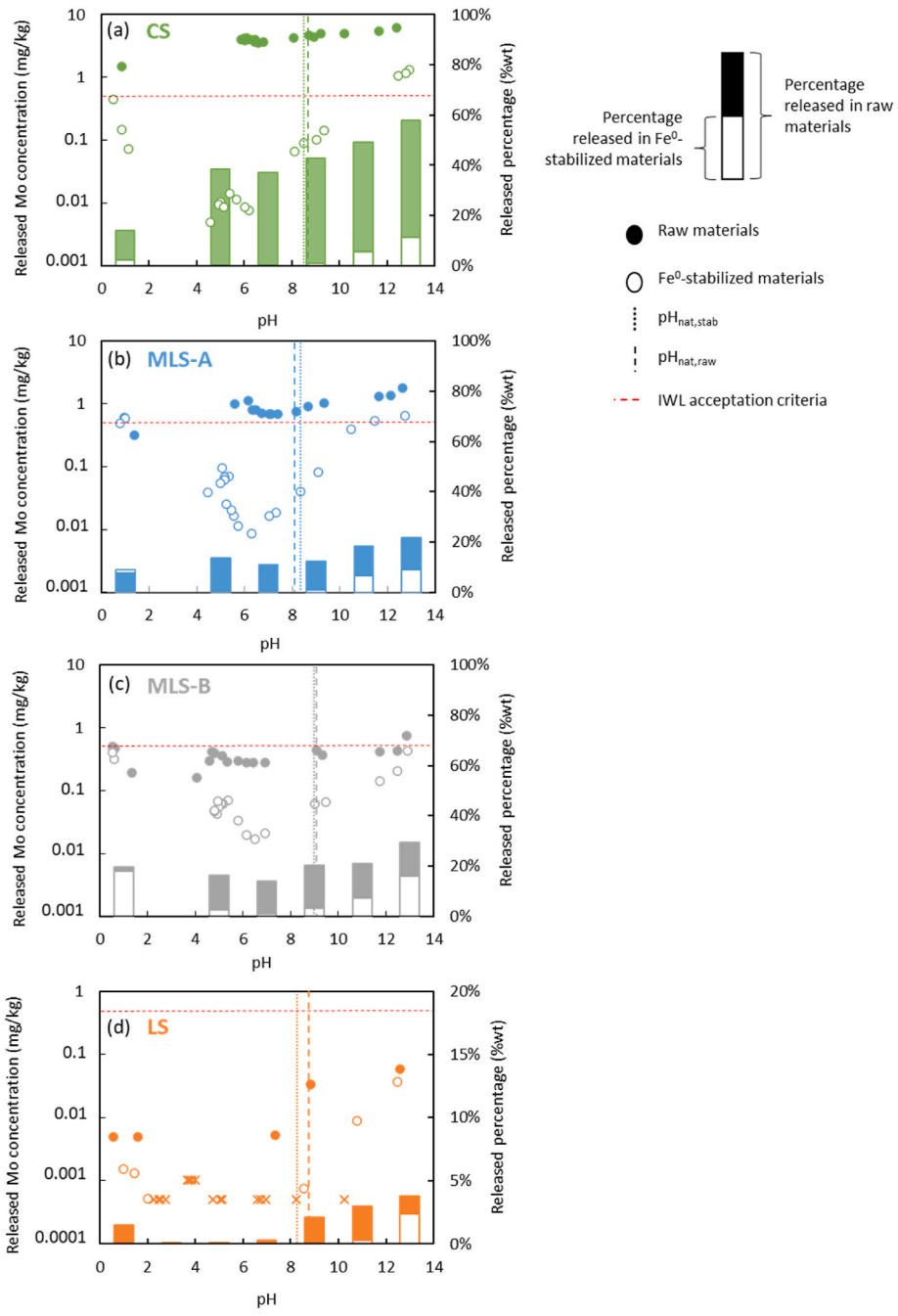

Fig. 1. Main y-axis - Comparison of Mo leaching patterns from raw materials (filled marks) and Fe^0-stabilized materials (empty marks) during pH-dependent leaching tests. Cross marks represent values below the Quantification Limit. Secondary y-axis - Mo released percentage calculated based on total content measured by ICP-MS.

material released a slightly higher quantity of Mo than raw material (Fig. 1b). Nevertheless, it was within the bounds of experimental uncertainty so both concentrations should be considered similar.

At natural batch pH (pH_{nat}), i.e. between pH 8 and 9, Mo release was significantly reduced by addition of Fe^0. A minimum difference with the release from raw samples of one order of magnitude was observed (Fig. 1). Mass balance calculation indicates that the fractions of total Mo released after Fe^0-stabilization became almost negligible. This was particularly clear for CS, for which total Mo released at pH_{nat} decreased from 43 wt% in an unstabilized sample to only 1 wt% in a Fe^0-stabilized sample. Decrease of Mo mobility was not limited to pH_{nat} so that significantly lower concentrations were measured in Fe^0-stabilized materials following both acid and base additions. Discrepancies were noticed between the different excavated materials. For example, Mo appeared to be strongly retained in the solid bulk in Fe^0-stabilized CS over the whole pH range with a release not exceeding 11 wt% of total Mo. On the other hand, under strongly acidic conditions, Mo leaching in Fe^0-stabilized MLS-A and ML-B were very close to the one obtained with a raw sample, which suggests a lower impact of stabilization in these samples. In the following sections, factors influencing these differences will be discussed in relation to the immobilizing mechanisms identified.

3.2. *Identification of stabilization mechanisms*

3.2.1. *Direct observations of stabilizing impact on Mo speciation*

Two Regions Of Interest (ROI) were selected on Fe^0-stabilized CS as

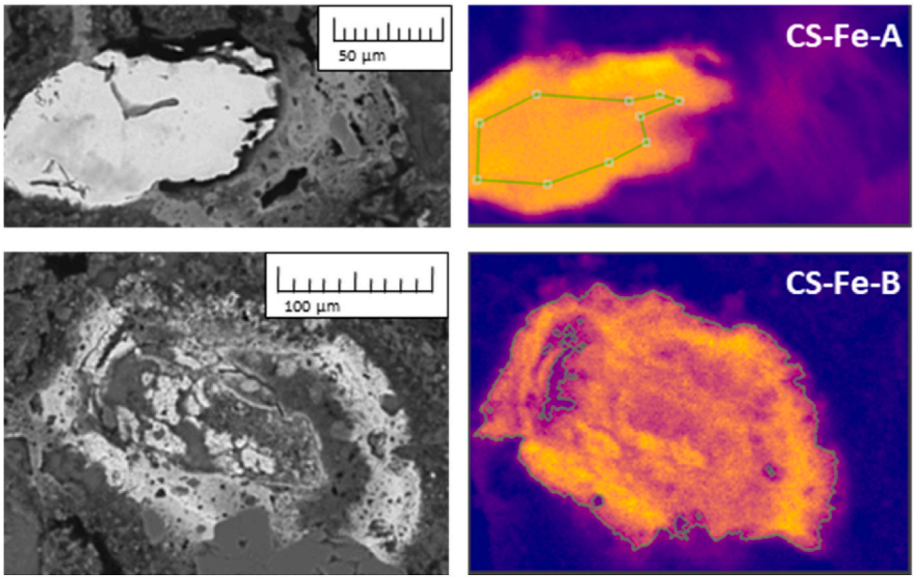

Fig. 2. SEM images and quantitative mapping of Fe distribution obtained with µ-PIXE measurements on two iron oxides grains selected in Fe^0-stabilized CS.

Table 2
Quantitative results obtained by µ-PIXE and µ-RBS on the two Regions Of Interest (ROI) shown in Fig. 2. For µ-RBS measurements of trace elements the Limit Of Detection (LOD) is given. O/Fe represents the weight ratio of Oxygen and Iron in the considered ROI.

	C	O	Ca	Fe	Mo	LOD Mo	O/Fe
Unit	wt.%	wt.%	wt.%	wt.%	$mg.kg^{-1}$	$mg.kg^{-1}$	–
CS-Fe-A	0	0	0	100	0	74	0
CS-Fe-B	16.6	29.5	1.8	53.9	141	60	0.55

they presented two different stages of zero valent iron grains-oxidation process (Fig. 2). The first ROI, CS-Fe-A, consisted of a pristine Fe^0 grain, as shown by the absence of other elements such as O, which could have served as an indicator of oxidation or C and Ca, which might have been detected given the high proportion of carbonated mineral in this sample (Table 2). On the other hand, CS-Fe-B consisted of iron (hydr-)oxides formed after Fe^0 oxidation. The mass percentage ratio O/Fe calculated (0.55) was higher and lower than the values expected for hematite (0.43) and ferrihydrite respectively (between 0.69 and 0.81 depending on the hydration state) but consistent with the one expected for goethite (0.57). The evaluated concentrations of Mo, over the limits of detection obtained with µ-PIXE measurements confirmed the presence of Mo associated with goethite in CS-Fe-B. The absence of both trace elements on the pristine Fe^0 grain (CS–Fe-A) supported the importance of oxidation to favor complexation phenomena by creating surface sites likely to be protonated (Cundy et al., 2008; Komárek et al., 2013). It also confirmed that the added Fe^0 was not completely converted into iron (hydr-)oxides inferring that further oxidation might slowly provide additional reactive surface sites likely to be involved in complexation mechanisms.

3.2.2. *Geochemical modeling*

Figures in SI (Fig. SI–2 to Fig. SI–6) show experimental and modeling results for pH-dependent leaching tests for general parameters (pH and conductivity), and major element concentrations for both raw and Fe^0-stabilized materials. For major elements, experimental data obtained from stabilized materials were very close to the one obtained from raw samples. The main exception logically concerned Fe concentration evolutions, which were seen to differ significantly between raw and stabilized materials due to Fe^0 addition (see indices *(e)* of Fig. SI–3 to SI-6). Based on the maximum Fe concentration released at pH < 2 for Fe^0-stabilized materials, a consistent fit was obtained for each sample considering that 80 % of the added Fe^0 was converted into iron (hydr-) oxides. Goethite was chosen to represent Fe^0 oxidation products in mainly carbonated samples (CS, MLS-A and MLS-B) according to nuclear microprobe analysis. For Fe^0-stabilized LS, evolution of Fe concentrations (Fig. SI–6e) and pH (Fig. SI–2g) during pH-dependent leaching tests were better described by taking ferrihydrite ($Fe(OH)_3$) into account.

Figs. 3 and 4 show experimental and modeling results for the evolution of Mo concentrations during pH-dependent leaching tests for all samples. First, it should be noted that addition of iron (hydr-)oxides to raw materials' geochemical models resulted in significant changes of Mo leaching behavior. For all samples, a decrease of Mo released concentrations was observed at pH values of 10 and below. No precipitation of the two considered ferromolybdate mineral phases (*i.e.* $FeMoO_4$ and $Fe_2(MoO_4)_3$) was observed, both remaining largely under saturated in the whole pH range. Molybdenum precipitation was therefore ruled out as a potential mechanism behind changes in Mo reactivity after Fe^0 addition, although this could have been expected because of the very low initial total content of Mo measured in all materials and given that ferrous molybdate precipitation was seen to require much higher Mo concentrations (Hem, 1977). The observed changes of Mo global mobility at pH < 10 were attributed to complexation enhancement due to the multiplication of surface reactive sites. Indeed, surface sites protonation increased with the decrease of pH so that retention of negatively charged species like MoO_4^{2-} ions was favored (van der Sloot and Dijkstra, 2004).

The representation of experimental data could be considered as satisfactory at pH values below 5, especially for Fe^0-stabilized MLS-A, MLS-B and LS, while Mo release appeared to be still slightly overestimated in the case of CS. The formation of the bi-protonated Mo surface species ($Hfo\_OMo(OH)_5$) was enhanced compared to raw materials because of the increasing number of surface sites as well as the positive charge induced by acid addition. However, at pH > 5, the decrease of Mo leaching obtained with modeling, due to complexation enhancement, was not significant enough to be taken into account. The integration of a mono-protonated Mo sorbed species ($Hfo\_MoO_4^-$) as defined by Dzombak and Morel (1990) was first inferred to have no impact on Mo leaching behavior. Nevertheless, it should be noted that its formation (red curves in Figs. 3 and 4) was centered on a maximum value reached at pH ≈ 7.4 for all samples. At such pH values, Mo-released concentrations were particularly overestimated by the

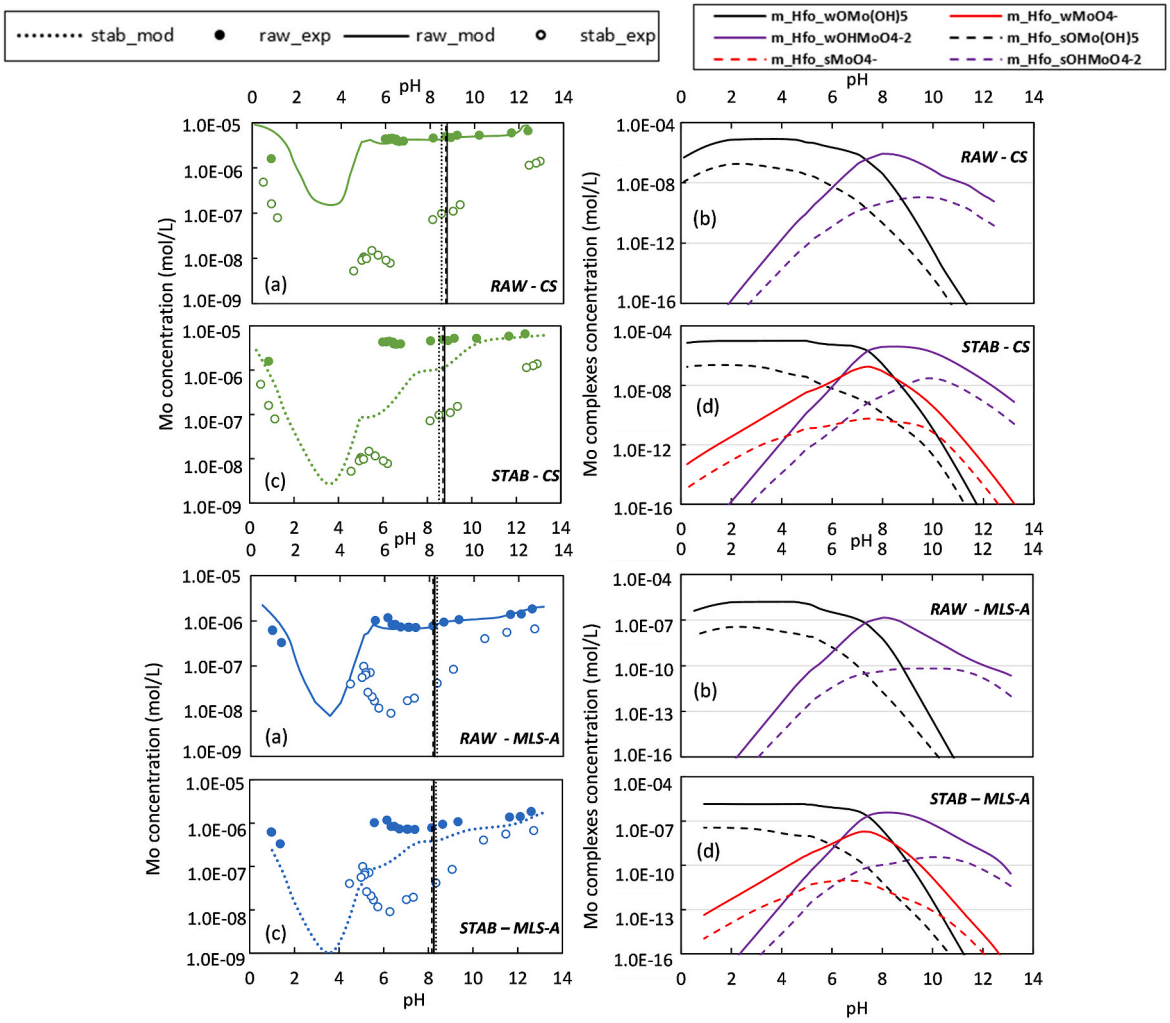

Fig. 3. Evolution of Mo concentration during pH-dependent leaching tests in raw (raw_exp, filled marks) and Fe^0-stabilized (stab_exp, empty marks) CS (green) and MLS-A (blue). Modeling results of Mo concentrations (raw_mod and stab_mod) and concentrations of Mo surface species are given on the left-hand side and on the right-hand side respectively. RAW (a and b): no addition of stabilizing agent (Case 1); STAB (c and d): addition of iron (hydr-)oxides (80 % of the quantity of Fe^0 added) and consideration of three Mo surface species (non-, mono- and bi-protonated) without optimization of formation constants (Case 2). (For interpretation of the references to colour in this figure legend, the reader is referred to the Web version of this article.)

modeling scenario. Consequently we considered that a stronger affinity for the formation of mono-protonated complexes could be a promising optimization tool for improving the representation of experimental observations.

To better constrain the models, an optimization of thermodynamic constants associated with Mo surface species formation reactions was implemented. Although other adjustable parameters could have been considered, the focus was on the surface complexation constants due to the uncertainty of integrating a mono-protonated Mo sorbed species in the models. To achieve this, a three-step optimization using Phreeplot software (Kinniburgh and Cooper, 2011) was carried out. The first step involved finding an optimal value for the mono-protonated complex while constants for the non- and bi-protonated complexes were left as compiled by Gustafsson (2003). This procedure was carried out using geochemical models of Fe^0-stabilized CS, MLS-A and MLS-B. The loam sample (LS) was not considered given the high proportion of Mo concentrations measured below the Quantification Limit (QL). Then, two more steps were carried out to see whether the optimization of thermodynamic constants for bi-protonated and non-protonated complexes could also improve the representation of Mo reactivity. The optimization process is presented graphically in SI (Fig. SI–7 to SI-9) while the resulting formation constants are summarized in Table 3.

The calculated thermodynamic constants were consistent between the three considered materials (Fe^0-stabilized CS, MLS-A and MLS-B). The optimization significantly improved the representation of experimental data by the geochemical model as confirmed by the decrease of the Root Mean Square Error (RMSE) and the increase of the determination coefficient (Fig. SI–7 to Fig. SI–9). In all cases, the strongest change was seen for the formation constant of the mono-protonated complex with a three-log unit difference. The two other complexes (non and bi-protonated) formation constants were only slightly modified, but still led to further improvements in the modeling of experimental data. Based on these observations, a final attempt was made to model Mo released concentrations from Fe^0-stabilized materials during pH-dependent leaching tests by using the mean values obtained for each Mo surface species (Case 3). The corresponding modeling results are given for CS and MLS-A in Fig. 5 and for MLS-B and LS in Fig. 6 and compared with the leaching behavior obtained from raw materials (solid curves). For each pH-dependent leaching curve obtained from Fe^0-stabilized samples (dotted curves), an area plot is given to represent the distribution of Mo between solid and liquid phases as suggested by the modeling results. The mass balances were calculated using Mo total content in each sample considering the difference between Mo total content and the quantity incorporated in the geochemical model as an

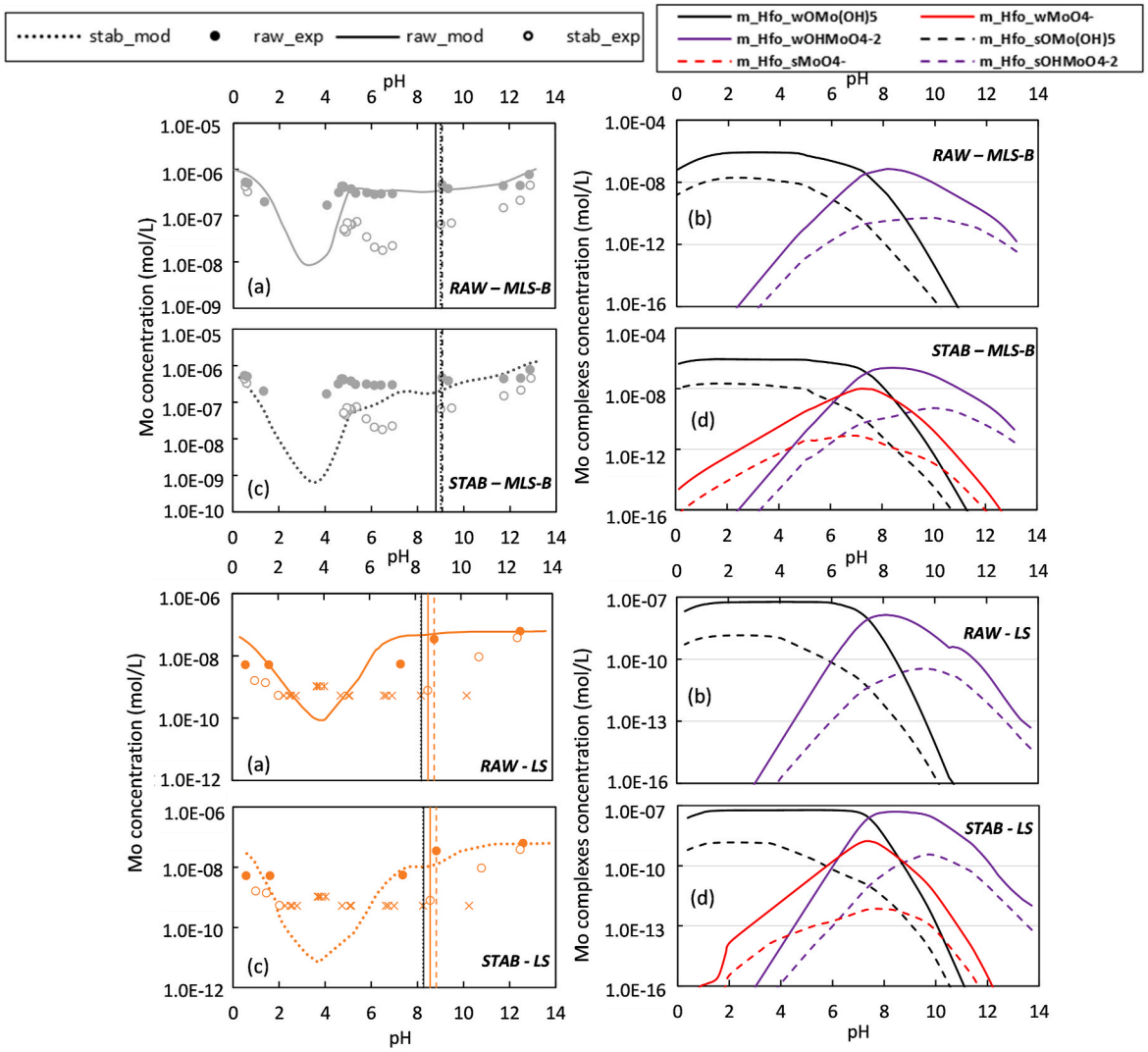

Fig. 4. Evolution of Mo concentration during pH-dependent leaching tests in raw (raw_exp, filled marks) and Fe^0-stabilized (stab_exp, empty marks) MLS-B (grey) and LS (orange). Modeling results of Mo concentrations (raw_mod and stab_mod) and concentrations of Mo surface species are given on the left-hand side and on the right-hand side respectively. RAW (a and b): no addition of stabilizing agent (Case 1); STAB (c and d): addition of iron (hydr-)oxides (80 % of the quantity of Fe^0 added) and consideration of three Mo surface species (non-, mono- and bi-protonated) without optimization of formation constants (Case 2). (For interpretation of the references to colour in this figure legend, the reader is referred to the Web version of this article.)

Table 3
Optimized thermodynamic constants for the three considered complexation reactions between Mo and iron (hydr-)oxides surfaces sites (Hfo) in Fe^0 stabilized samples. Optimization was carried out using Phreeplot (Kinniburgh and Cooper, 2011). C_1 = Hfo_OHMoO$_4^{2-}$; C_2 = Hfo_MoO$_4^-$; C_3 = Hfo_OMo(OH)$_5$; *This study.

	Log_k C_1	Log_k C_2	Log_k C_3
Dzombak and Morel (1990)	2.5	9.5	–
Gustafsson (2003)	3.14	–	17.96
CS*	4.25	12.98	18.70
MLS-A*	4.15	12.84	17.40
MLS-B*	4.05	12.13	17.13
Mean value*	4.15 ± 0.10	12.59 ± 0.46	17.76 ± 0.84

unreactive fraction under pH-dependent leaching test conditions (dark grey areas).

In LS, Mo was initially mainly in unreactive forms with approximatively 95 wt% of total Mo inferred to be strongly associated with the solid bulk, which was consistent with the very low mobility observed. Despite the particular behavior and initial speciation of Mo in LS, modeling results using the optimized complexation constants allowed a fair representation of Mo release, especially at pH < pH_{nat} where concentrations fell down below the QL. In the mainly carbonated samples, modeling of Fe^0-stabilization, considering that complexation phenomena played a major role, also resulted in satisfactory representation of experimental data at pH < pH_{nat}. First, it should be noted that the Mo release at the natural pH was faithfully reflected in modeling results for all materials. This might be of interest since these conditions were close to the one occurring in standardized batch leaching tests and it might therefore help predict the efficiency of the stabilizing solution regarding the compliance of inert waste landfill acceptance criteria. From the area plots shown in Figs. 5 and 6, it could be inferred that Mo mobility at pH_{nat} was strongly mitigated by the formation of a mixture of non- and mono-protonated complexes.

Molybdenum (Mo) complexation at iron (hydr-)oxides surfaces was shown to prevail in Fe^0-stabilized materials when pH decreased with a leaching pattern well described by geochemical modeling. However, on the other side of the pH range, the same discrepancies between modeling and experimental data were observed for all materials. According to the modeling results, Mo concentrations progressively increased with

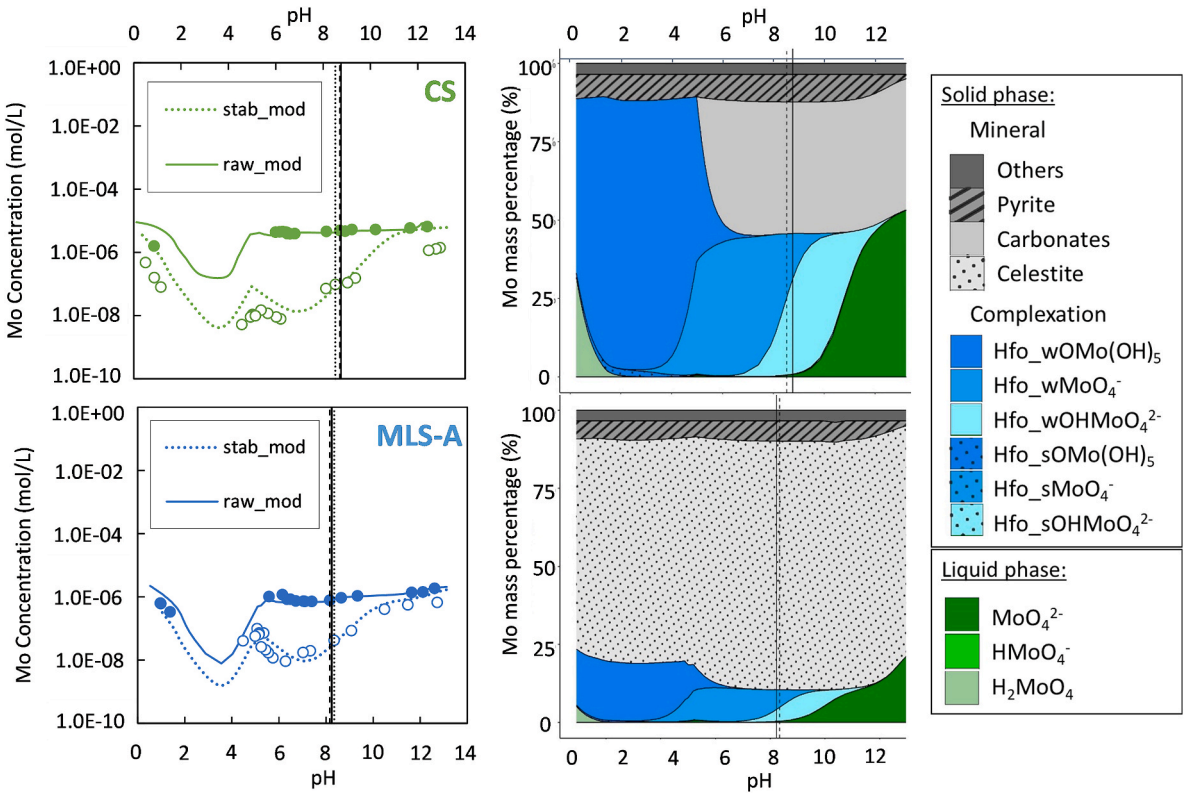

Fig. 5. Evolution of Mo concentration during pH-dependent leaching tests carried out on raw (filled marks) and Fe^0-stabilized (empty marks) CS and MLS-A. Both experimental (marks) and modeling (lines, raw_mod and stab_mod respectively for raw and Fe^0-stabilized materials) results are presented. Modeled curves for raw materials (raw_mod, solid lines) were obtained in a previous work (Brandely et al., 2022a). Vertical dashed and dotted lines represent the experimental natural batch pH for raw and Fe^0-stabilized samples respectively while vertical solid lines represent modeled natural batch pH. Cross marks represent values below the Quantification Limit. Area plots on the right hand side of the figure represent Mo distribution between solid and liquid phases in Fe^0-stabilized samples as suggested by geochemical models. Mass balances were calculated using Mo total content measured by ICP-MS.

addition of base because of successive desorption of Mo from iron (hydr-)oxides and partial dissolution of Mo-bearing mineral phases (celestite, dolomite and pyrite). The results showed that Mo leaching patterns of Fe^0-stabilized materials were ultimately confounded with that of raw materials. Nevertheless, experimental results have shown a persistence of Mo immobilization even at the highest pH values. The inference is that of a relative stability of immobilization mechanisms, since alkaline pH conditions are highly unfavorable for the retention of negatively charged species, especially through complexation at oxides surfaces (van der Sloot and Dijkstra, 2004). Given that Fe^0 addition was not expected to affect the behavior of Mo-bearing phases and that no other stabilizing mechanisms were suspected, the difference between experimental and modeling results might rather be due to uncompleted desorption. Compared to adsorption, Mo desorption mechanisms are poorly understood (Sun and Selim, 2020). Yet, regular deviations between adsorption and desorption patterns have been acknowledged either when performing Mo adsorption studies on raw materials (Lang and Kaupenjohann, 2003) or on iron oxides coated with sand (Sun and Selim, 2018, 2019). Several assumptions were suggested to explain these hysteresis-like phenomena such as the two-step desorption process based on (i) fast release of Mo sorbed at reactive surface sites and (ii) slow release due to diffusion out of oxide crystalline structures. It might also be advanced that some of the adsorbed Mo was actually precipitated at the surface of iron (hydr-)oxides. It is known that surface complexation and surface precipitation mechanisms are difficult to distinguish from each other (Young, 2013). The stronger binding involved with the latter could result in irreversible desorption.

4. Conclusion

The mobility of molybdenum in naturally contaminated excavated materials is significantly reduced by reasonably low addition of zero valent iron (<3 wt%) over a wide pH range. Coupling pH-dependent leaching test results with geochemical modeling suggests an immobilizing pathway involving complexation at iron (hydr-)oxide surfaces. The inference from modeling results was that three Mo surface species could be pH-dependent with, respectively, non-, mono- and bi-protonated Mo complexes. The use of nuclear microprobe analysis identified Mo in association with iron (hydr-)oxides formed during Fe^0 oxidation.

Complexation at iron (hydr-)oxide surfaces due to Fe^0 addition appeared to be resilient to pH variations with respect to soil acidification as well as alkalinization. However, further studies should be carried out to determine whether Mo immobilization would resist stronger weathering conditions that might mimic evolution of excavated materials in a long-term storage or reuse scenario.

CRediT authorship contribution statement

Maxime Brandely: Writing – original draft, Methodology, Investigation, Formal analysis, Data curation, Conceptualization. **Samuel Coussy:** Writing – review & editing, Supervision, Project administration, Methodology, Investigation, Funding acquisition, Formal analysis, Data curation, Conceptualization. **Denise Blanc-Biscarat:** Writing – review & editing, Supervision, Conceptualization. **Hicham Khodja:** Writing – review & editing, Investigation, Formal analysis, Data curation. **Rémy Gourdon:** Writing – review & editing, Supervision, Conceptualization.

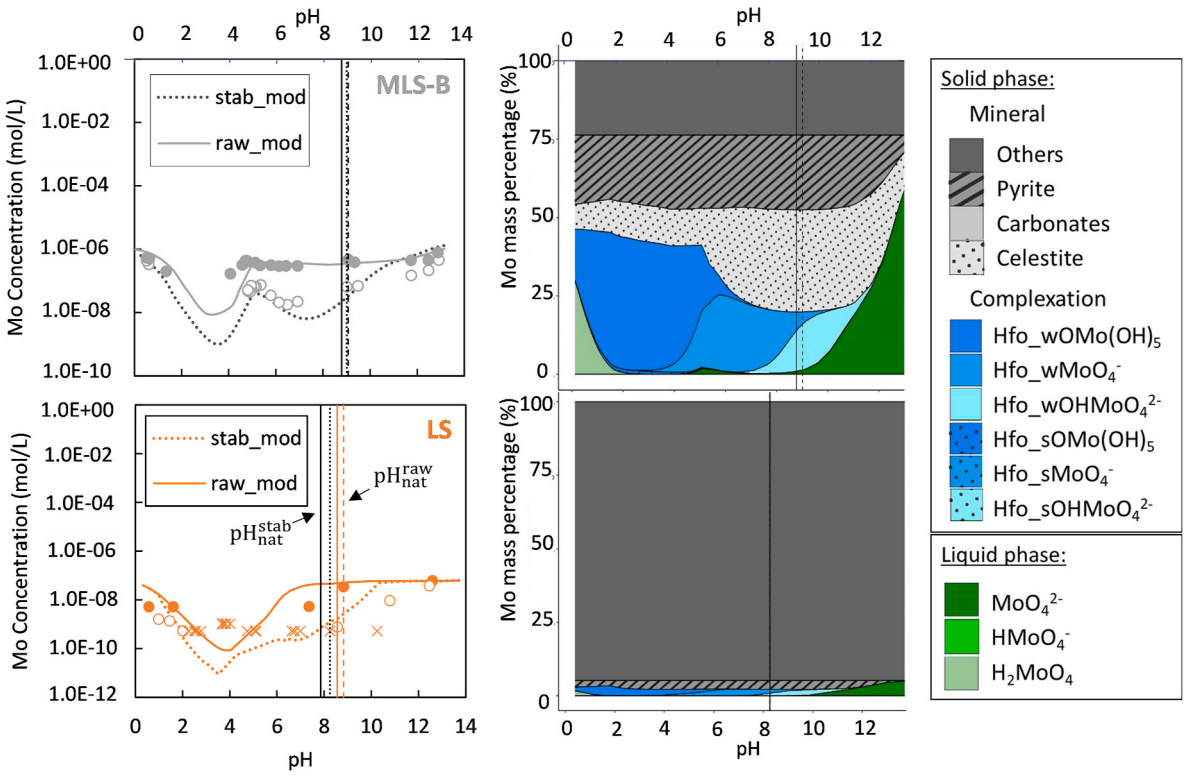

Fig. 6. Evolution of Mo concentration during pH-dependent leaching tests carried out on raw (filled marks) and Fe^0-stabilized (empty marks) MLS-B and LS. Both experimental (marks) and modeling (lines, raw_mod and stab_mod respectively for raw and Fe^0-stabilized materials) results are presented. Modeled curves for raw materials (raw_mod, solid lines) were obtained in a previous work (Brandely et al., 2022a). Vertical dashed and dotted lines represent the experimental natural batch pH for raw and Fe^0-stabilized samples respectively while vertical solid lines represent modeled natural batch pH. Cross marks represent values below the Quantification Limit. Area plots on the right hand side of the figure represent Mo distribution between solid and liquid phases in Fe^0-stabilized samples as suggested by geochemical models. Mass balances were calculated using Mo total content measured by ICP-MS.

Declaration of competing interest

The authors declare the following financial interests/personal relationships which may be considered as potential competing interests: Maxime Brandely reports financial support was provided by Bouygues Travaux Publics SAS. If there are other authors, they declare that they have no known competing financial interests or personal relationships that could have appeared to influence the work reported in this paper.

Acknowledgements

The authors would like to thank the staff of the (LEEL) for the opportunity to use the nuclear microprobe facility in Saclay (France). Scanning Electron Microscopy prior to nuclear microprobe analysis was carried out at BRGM (Orléans, France) with the much-appreciated help of C. Duée. The authors are also grateful to T. Conte and the BRGM laboratory team, who performed all liquid analyses following pH-dependent leaching tests. Finally, we would like to thank the Central Laboratory of *Bouygues Travaux Publics* for having provided the raw and stabilized materials. This study was financially supported by *Bouygues Travaux Publics* (France) as a part of the IMMOTERRE research and development project.

Appendix A. Supplementary data

Supplementary data to this article can be found online at https://doi.org/10.1016/j.apgeochem.2025.106433.

Data availability

The data that has been used is confidential.

References

Beiyuan, J., Tsang, D.C.W., Ok, Y.S., Zhang, W., Yang, X., Baek, K., Li, X.-D., 2016. Integrating EDDS-enhanced washing with low-cost stabilization of metal-contaminated soil from an e-waste recycling site. Chemosphere 159, 426–432. https://doi.org/10.1016/j.chemosphere.2016.06.030.

Brandely, M., Coussy, S., Blanc-Biscarat, D., Gourdon, R., 2022a. Assessment of Molybdenum and Antimony speciation in excavated rocks and soils from the Parisian basin using mineralogical and chemical analyses coupled to geochemical modelling. Appl. Geochem. 136, 105129. https://doi.org/10.1016/j.apgeochem.2021.105129.

Brandely, M., Coussy, S., Blanc-Biscarat, D., Gourdon, R., Blanck, G., 2022b. Chemical stabilization used to reduce geogenic selenium, molybdenum, sulfates and Fluorides mobility in rocks and soils from the parisian basin. Environments 9, 78. https://doi.org/10.3390/environments9070078.

Cabrerizo, A., Bulteel, D., Waligora, J., Landrot, G., Fonda, E., Olard, F., 2020. Chemical, mineralogical, and environmental characterization of tunnel boring muds for their valorization in road construction: a focus on molybdenum characterization. Environ. Sci. Pollut. Res. https://doi.org/10.1007/s11356-020-09969-6.

Calugaru, I.L., Etteieb, S., Magdouli, S., Genty, T., 2021. Selenium-rich mine effluents treatment using zero-valent iron: Mechanism and removal efficiency in the cold climate of Québec, Canada. Environ. Adv. 5, 100099. https://doi.org/10.1016/j.envadv.2021.100099.

Coussy, S., Benzaazoua, M., Blanc, D., Moszkowicz, P., Bussière, B., 2011. Arsenic stability in arsenopyrite-rich cemented paste backfills: a leaching test-based assessment. J. Hazard Mater. 185, 1467–1476. https://doi.org/10.1016/j.jhazmat.2010.10.070.

Cundy, A.B., Hopkinson, L., Whitby, R.L.D., 2008. Use of iron-based technologies in contaminated land and groundwater remediation: a review. Sci. Total Environ. 400, 42–51. https://doi.org/10.1016/j.scitotenv.2008.07.002.

Diaz Caselles, L., Roosz, C., Hot, J., Blotevogel, S., Cyr, M., 2021. Immobilization of molybdenum by alternative cementitious binders and synthetic C-S-H: an experimental and numerical study. Sci. Total Environ. 789, 148069. https://doi.org/10.1016/j.scitotenv.2021.148069.

Drapeau, C., 2018. Mesure et modélisation de la mobilité et de la spéciation des éléments majeurs et traces métalliques au sein de matrices complexes polluées en fonction du pH : application aux sédiments urbains et déchets miniers (phdthesis). Université de Lyon.

Dzombak, D.A., Morel, F.M.M., 1990. Surface Complexation Modeling: Hydrous Ferric Oxide. John Wiley & Sons.

Giffaut, E., Grivé, M., Blanc, Ph, Vieillard, Ph, Colàs, E., Gailhanou, H., Gaboreau, S., Marty, N., Madé, B., Duro, L., 2014. Andra thermodynamic database for performance assessment: ThermoChimie. Appl. Geochem. Geochem. Risk Assess.: Hazardous waste in the Geosphere 49, 225–236. https://doi.org/10.1016/j.apgeochem.2014.05.007.

Guan, X., Sun, Y., Qin, H., Li, J., Lo, I.M.C., He, D., Dong, H., 2015. The limitations of applying zero-valent iron technology in contaminants sequestration and the corresponding countermeasures: the development in zero-valent iron technology in the last two decades (1994–2014). Water Res. 75, 224–248. https://doi.org/10.1016/j.watres.2015.02.034.

Gustafsson, J.P., 2003. Modelling molybdate and tungstate adsorption to ferrihydrite. Chem. Geol. 200, 105–115. https://doi.org/10.1016/S0009-2541(03)00161-X.

Gustafsson, J.P., Tiberg, C., 2015. Molybdenum binding to soil constituents in acid soils: an XAS and modelling study. Chem. Geol. 417, 279–288. https://doi.org/10.1016/j.chemgeo.2015.10.016.

Hartley, W., Edwards, R., Lepp, N.W., 2004. Arsenic and heavy metal mobility in iron oxide-amended contaminated soils as evaluated by short- and long-term leaching tests. Environ. Pollut. 131, 495–504. https://doi.org/10.1016/j.envpol.2004.02.017.

Hem, J.D., 1977. Reactions of metal ions at surfaces of hydrous iron oxide. Geochem. Cosmochim. Acta 41, 527–538. https://doi.org/10.1016/0016-7037(77)90290-3.

Hiemstra, T., Van Riemsdijk, W.H., 1996. A surface structural approach to ion adsorption: the charge distribution (CD) model. J. Colloid Interface Sci. 179, 488–508. https://doi.org/10.1006/jcis.1996.0242.

Houben, D., Pircar, J., Sonnet, P., 2012. Heavy metal immobilization by cost-effective amendments in a contaminated soil: effects on metal leaching and phytoavailability. J. Geochem. Explor. Phytoremediation pollut. soil 123, 87–94. https://doi.org/10.1016/j.gexplo.2011.10.004.

Khalid, S., Shahid, M., Niazi, N.K., Murtaza, B., Bibi, I., Dumat, C., 2017. A comparison of technologies for remediation of heavy metal contaminated soils. J. Geochem. Explor. Remed. Pollut. Soils Part 2 182, 247–268. https://doi.org/10.1016/j.gexplo.2016.11.021.

Khodja, H., Berthoumieux, E., Daudin, L., Gallien, J.-P., 2001. The Pierre Süe Laboratory nuclear microprobe as a multi-disciplinary analysis tool. Nucl. Instrum. Methods Phys. Res., Sect. B: Beam Interact. Mater. Atoms 7th Int. Conf. Nuclear Microprobe Technol. Appl. 181, 83–86. https://doi.org/10.1016/S0168-583X(01)00564-X.

Kinniburgh, David, Cooper, David, 2011. PhreePlot: Creating graphical output with PHREEQC [Software user manual].

Komárek, M., Vaněk, A., Ettler, V., 2013. Chemical stabilization of metals and arsenic in contaminated soils using oxides – a review. Environ. Pollut. 172, 9–22. https://doi.org/10.1016/j.envpol.2012.07.045.

Kumpiene, J., Ore, S., Renella, G., Mench, M., Lagerkvist, A., Maurice, C., 2006. Assessment of zerovalent iron for stabilization of chromium, copper, and arsenic in soil. Environ. Pollut. Soil Sediment Remed. (SSR) 144, 62–69. https://doi.org/10.1016/j.envpol.2006.01.010.

Lang, F., Kaupenjohann, M., 2003. Immobilisation of molybdate by iron oxides: effects of organic coatings. Geoderma 113, 31–46. https://doi.org/10.1016/S0016-7061(02)00314-2.

Mancini, G., Palmeri, F., Luciano, A., Viotti, P., Fino, D., 2020. Partial stabilization of Mo-containing hazardous wastes using a ferrous sulfate-based additive as a redox agent. Waste Biomass Valor 11, 5493–5502. https://doi.org/10.1007/s12649-020-01095-1.

Marty, N.C.M., Claret, F., Lassin, A., Tremosa, J., Blanc, P., Madé, B., Giffaut, E., Cochepin, B., Tournassat, C., 2015. A database of dissolution and precipitation rates for clay-rocks minerals. Applied Geochemistry, Geochemical Speciation Codes and Databases 55, 108–118. https://doi.org/10.1016/j.apgeochem.2014.10.012.

Mench, M., Vangronsveld, J., Beckx, C., Ruttens, A., 2006. Progress in assisted natural remediation of an arsenic contaminated agricultural soil. Environ. Pollut. 144, 51–61. https://doi.org/10.1016/j.envpol.2006.01.011.

NF EN ISO 17294-2 - AFNOR, 2016. Water quality — application of inductively coupled plasma mass spectrometry (ICP-MS) — Part 2: determination of selected elements including uranium isotopes. https://www.boutique.afnor.org/en-gb/standard/nf-en-iso-172942/water-quality-application-of-inductively-coupled-plasma-mass-spectrometry-i/fa180689/58002.

NF EN 14429 - AFNOR, 2015. Characterization of waste — leaching behaviour test — influence of pH on leaching with initial acid/base addition. https://www.boutique.afnor.org/fr-fr/norme/nf-en-14429/caracterisation-des-dechets-essais-de-comportement-a-la-lixiviation-influen/fa181002/45654.

NF EN 12457-2 - AFNOR, 2002. Characterization of waste - leaching - Compliance test for leaching of granular waste materials and sludges - Part 2 : one stage batch test at a liquid to solid ratio of 10 l/kg for materials with particle size below 4 mm (without or with size reduction). https://www.boutique.afnor.org/en-gb/standard/nf-en-124572/characterization-of-waste-leaching-compliance-test-for-leaching-of-granular/fa104282/20764.

Official Journal of the European Union (OJEC), 2003. 2003/33/EC: council Decision of 19 December 2002 establishing criteria and procedures for the acceptance of waste at landfills pursuant to Article 16 of and Annex II to Directive 1999/31/EC. https://eur-lex.europa.eu/eli/dec/2003/33(1)/oj/eng.

Palansooriya, K.N., Shaheen, S.M., Chen, S.S., Tsang, D.C.W., Hashimoto, Y., Hou, D., Bolan, N.S., Rinklebe, J., Ok, Y.S., 2020. Soil amendments for immobilization of potentially toxic elements in contaminated soils: a critical review. Environ. Int. 134, 105046. https://doi.org/10.1016/j.envint.2019.105046.

Parkhurst, D.L., Appelo, C.A.J., 2013. Description of input and examples for PHREEQC version 3: a computer program for speciation, batch-reaction, one-dimensional transport, and inverse geochemical calculations (USGS Numbered Series No. 6-A43), Description of input and examples for PHREEQC version 3: a computer program for speciation, batch-reaction, one-dimensional transport, and inverse geochemical calculations. In: Techniques and Methods. U.S. Geological Survey, Reston, VA. https://doi.org/10.3133/tm6A43.

Sterckeman, T., Douay, F., Baize, D., Fourrier, H., Proix, N., Schvartz, C., 2006. Trace elements in soils developed in sedimentary materials from Northern France. Geoderma 136, 912–929. https://doi.org/10.1016/j.geoderma.2006.06.010.

Sun, W., Selim, H.M., 2020. Chapter Two - fate and transport of molybdenum in soils: kinetic modeling. In: Sparks, D.L. (Ed.), Advances in Agronomy. Academic Press, pp. 51–92. https://doi.org/10.1016/bs.agron.2020.06.002.

Sun, W., Selim, H.M., 2019. Kinetic modeling of pH-dependent molybdenum(VI) adsorption and desorption on iron oxide-coated sand. Soil Sci. Soc. Am. J. 83, 357–365. https://doi.org/10.2136/sssaj2018.11.0449.

Sun, W., Selim, H.M., 2018. Kinetics of molybdenum adsorption and desorption in soils. J. Environ. Qual. 47, 504–512. https://doi.org/10.2134/jeq2018.01.0013.

Tabelin, C.B., Hashimoto, A., Igarashi, T., Yoneda, T., 2014. Leaching of boron, arsenic and selenium from sedimentary rocks: I. Effects of contact time, mixing speed and liquid-to-solid ratio. Sci. Total Environ. 472, 620–629. https://doi.org/10.1016/j.scitotenv.2013.11.006.

Tiberg, C., Kumpiene, J., Gustafsson, J.P., Marsz, A., Persson, I., Mench, M., Kleja, D.B., 2016. Immobilization of Cu and as in two contaminated soils with zero-valent iron – long-term performance and mechanisms. Appl. Geochem. 67, 144–152. https://doi.org/10.1016/j.apgeochem.2016.02.009.

van der Sloot, H., Dijkstra, J., 2004. Development of horizontally standardized leaching tests for construction materials: a material or release based approach? Identical leaching mechanisms for different materials. https://doi.org/10.13140/RG.2.2.11986.76486.

Vollprecht, D., Krois, L.-M., Sedlazeck, K.P., Müller, P., Mischitz, R., Olbrich, T., Pomberger, R., 2019. Removal of critical metals from waste water by zero-valent iron. J. Clean. Prod. 208, 1409–1420. https://doi.org/10.1016/j.jclepro.2018.10.180.

Wang, X., Brunetti, G., Tian, W., Owens, G., Qu, Y., Jin, C., Lombi, E., 2021. Effect of soil amendments on molybdenum availability in mine affected agricultural soils. Environ. Pollut. 269, 116132. https://doi.org/10.1016/j.envpol.2020.116132.

Young, S.D., 2013. Chemistry of heavy metals and metalloids in soils. In: Alloway, B.J. (Ed.), Heavy Metals in Soils: Trace Metals and Metalloids in Soils and Their Bioavailability, Environmental Pollution. Springer, Netherlands, Dordrecht, pp. 51–95. https://doi.org/10.1007/978-94-007-4470-7_3.

Yue, P., Chen, N., Peak, D., Bompoti, N.M., Chrysochoou, M., Onnis-Hayden, A., Larese-Casanova, P., 2020. Oxygen atom release during selenium oxyanion adsorption on goethite and hematite. Appl. Geochem. 117, 104605. https://doi.org/10.1016/j.apgeochem.2020.104605.